Universal Journal of Civil Engineering
https://ojs.wiserpub.com/index.php/UJCE/

Research Article

Teleconnection between the Low Index Phase of Southern Oscillation and Precipitation Patterns over the Southeastern United States

Seungho Lee*

South Carolina Lexington H. School, Lexington, SC, USA
E-mail: johnlee81282@gmail.com

Received: 31 July 2022; **Revised:** 2 October 2022; **Accepted:** 28 October 2022

Abstract: The purpose of this analysis is to examine the spatiotemporal extent to which the extreme phase of Southern Oscillation affects precipitation patterns over the southeastern region of the United States. Composite and harmonic analyses using monthly precipitation data were conducted based on the 2-year composite resulting in harmonic dials, which represent the spatial coherence of the candidate regions. For the candidate regions identified in the harmonic dial maps, aggregate composite and index time series of precipitation were analyzed to determine the core regions which represent the temporal consistency in relation to the low index phase of Southern Oscillation (LISO) events. As a result, the precipitation patterns of the core regions, Upper Region (UR), Middle Region (MR), and Lower Region (LR), were influenced by the occurrence of the extreme phase of SO events, with LR having the greatest response. During the LISO cycle, the harmonic dial tends to face southeast in UR, northeast in MR, and east in LR. Furthermore, the spatial coherence rates of the three core regions range from 0.94 to 0.99, and the temporal consistency rates are 0.76 to 0.83. In addition, from the cross-correlation and annual cycle analyses, the seasonal and annual effect of LISO forcing on the precipitation variability over the three core regions can be recognizable. In conclusion, Southern Oscillation phenomena have a great influence on the precipitation patterns over the southeastern region of the United States.

***Keywords*:** Precipitation; Southern oscillation; Teleconnection

1. Introduction

The Southern Oscillation (SO) is one of the well-known climate indicators, which represents large-scale fluctuations in sea level pressure over the western and eastern Pacific Ocean. These large-scale naturally occurring phenomena have been investigated at regional and global scales since the extreme phases of the SO episodes can cause major hydrologic extremes in various parts over the world. Many scientific approaches for understanding these phenomena have been providing us a chance to prepare for the disastrous hazards such as torrential rainstorm, floods, and droughts.

As a pioneering research, Walker and Bliss [1,2] studied firstly the impacts of the Southern Oscillation (SO) on the Indian precipitation variability. Since then, a number of global scale studies related to the SO extreme phases showed various notable climatic links between precipitation patterns and SO extreme events in many areas. Since Berlage [3] found the SO extreme events correlated well with precipitation anomaly on a global basis, Rasmusson and Carpenter [4] related the precipitation and temperature patterns to the extreme phase of Southern Oscillation and identified a significant link between the two variations. Ropelewski and Halpert [5,6] investigated temporal and spatial ranges showing consistent

DOI: https://doi.org/10.37256/ujce01010005

response of the precipitation pattern over a variety of areas throughout the world to the extreme phases of the SO episodes and showed significant correlations of the SO phase and precipitation patterns. More recently, Westra et al. [7] used generalized extreme value (GEV) to identify trends in annual maximum daily precipitation on a global basis and found a significant correlation with near-surface air temperature averaged globally.

For midlatitude regions, several studies indicated the SO–related precipitation correlation. For the southeastern United States, Douglas and Englehart [8] revealed that the extreme SO phase modulated the increases of the winter precipitation. Ropelewski and Halpert [9] studied the climatic links between the extreme southern oscillation and precipitation anomalies over North America and showed the SO-related precipitation signals. Cayan and Peterson [10], Redmond and Koch [11], Cayan and Web [12], and Diaz and Kiladis [13] investigated the influence of North Pacific atmospheric circulation on streamflow in the western United States. Kahya and Dracup [14,15] diagnosed the impacts of Southern Oscillation on U.S. streamflow patterns from the perspective of extratropical teleconnections triggered by tropical sea surface temperature variation. Grimm et al. [16] documented the influence of the extreme phase of SO on precipitation variability over southern Brazil using monthly precipitation data over 250 stations. Chiew et al. [17] examined the relationship between Southern Oscillation forcing and streamflow patterns in southeast Australia with an empirical methodology. In Turkey, some coherent regions where precipitation anomaly is statistically correlated with both phases of SO extreme events were founded by Karabörk and Kahya [18]. Also, they detected strong signal seasons and regions associated with the extreme phase of Southern Oscillation events [19]. Korea-Japan precipitation patterns were investigated by Jin et al. [20] in relation to the SO far-reaching effects. They used lead-lag correlation analysis for five categorized Southern Oscillation Index (SOI) and non-exceedance precipitation probability time series and showed evidence of the SO-precipitation correlation. In Sri Lanka, the Kelani River basin was examined by Chandimala and Zubair [21] focusing on the precipitation probability related to the SO and sea surface temperature using principal component and correlation analyses. A coupled general circulation model was employed by Power et al. [22] for investigating the climatic responses of Australian precipitation patterns to the SO forcing. Also, Cai et al. [23] examined the SO effects on the precipitation pattern over Australia in terms of extratropical and tropical teleconnections triggered by the equatorial the Pacific Sea surface temperature. Zhang et al. [24] confirmed variability and teleconnections between annual maximum streamflow of Yangtze River basin in China and Southern Oscillation by cross-wavelet analysis and wavelet coherence. Kashid et al. [25] examined hydroclimatic teleconnections between large-scale circulation patterns and streamflow in Mahanadi River, India using statistical techniques and Artificial Intelligence (AI) tools. Lee et al. [26-28] showed teleconnection of the two phases of SO forcing and midlatitude precipitation variability in the Korean peninsula, and Wang et al. [29] investigated the role of SO events in climatic links between Chinese precipitation patterns and tropical cyclones.

Despite the various research on the SO-related climate teleconnection, little is known about the perspective of the Low Index Phase of Southern Oscillation (LISO) on the localized precipitation variability. Recently, precipitation is occurring in more localized and intensified events and the corresponding hydrologic extremes have a devastating effect on people's lives, property, and the natural environment. Therefore, delving into the underlying local scale influences of the extreme phases of climatic variation on various scopes of precipitation patterns provides a constructive way to predict and prepare unexpected natural hazards. Thus, it is important to investigate systematically how the extreme phase of LISO events influence the local precipitation patterns over the middle latitude regions. Specifically, this study is to provide updated climate information of the temporal phase, spatial extent, and intensity of LISO-related precipitation signals over the study area. The objective of this study is to investigate precipitation variabilities over the middle latitude area associated with low index phase of extreme SO events using composite and harmonic analyses. This study uses an improved description by temporal cycle and spatial outlook for the intensity, time shift, and areal boundary of the LISO-precipitation correlation. Also, the present study examines seasonal and annual precipitation variation induced by the extreme phase of SO considering magnitude and trend of the significant responses, using annual cycle and cross-correlation analyses.

2. Data

The monthly precipitation time series used in this study are based on 45 climate divisions covering the entire southeast climate region. The source of the applied dataset is National Center for Environmental Information (NCEI) which is a governmental organization under the National Oceanic and Atmospheric Administration (NOAA). NOAA

monitors and operates the overall United States meteorology. As shown in Figure 1, the monthly precipitation data range from 1895 to 2020 and cover the overall 29 LISO episodes. To identify a consistent far-reaching effect of LISO events on precipitation anomaly over the southeastern United States, a set of extreme LISO episodes is selected considering a comprehensive scope of criteria defined by Ropelewski and Halpert [5,6], Rasmusson and Carpenter [4]. The event years for the extreme southern oscillation selected in the present analysis are listed in Table 1. Southern Oscillation Index (SOI) is applied as an indicator of representing large-scale climate variation over the central-eastern Pacific Ocean (ENSO). This present analysis applied the SOI data calculated and recorded by the NOAA Climate Prediction Center. These SOI time series are computed based on the difference of the standardized sea level pressure (SLP) anomaly between Tahiti and Darwin, Australia.

Table 1. List of the low index phase of southern oscillation (LISO) years

LISO years
1905, 1911, 1914, 1918, 1923, 1925, 1930, 1932, 1939, 1941, 1951, 1953, 1957, 1963, 1965, 1969, 1972, 1976, 1982, 1986, 1991, 1994, 1997, 2002, 2004, 2006, 2009,2015, 2018.

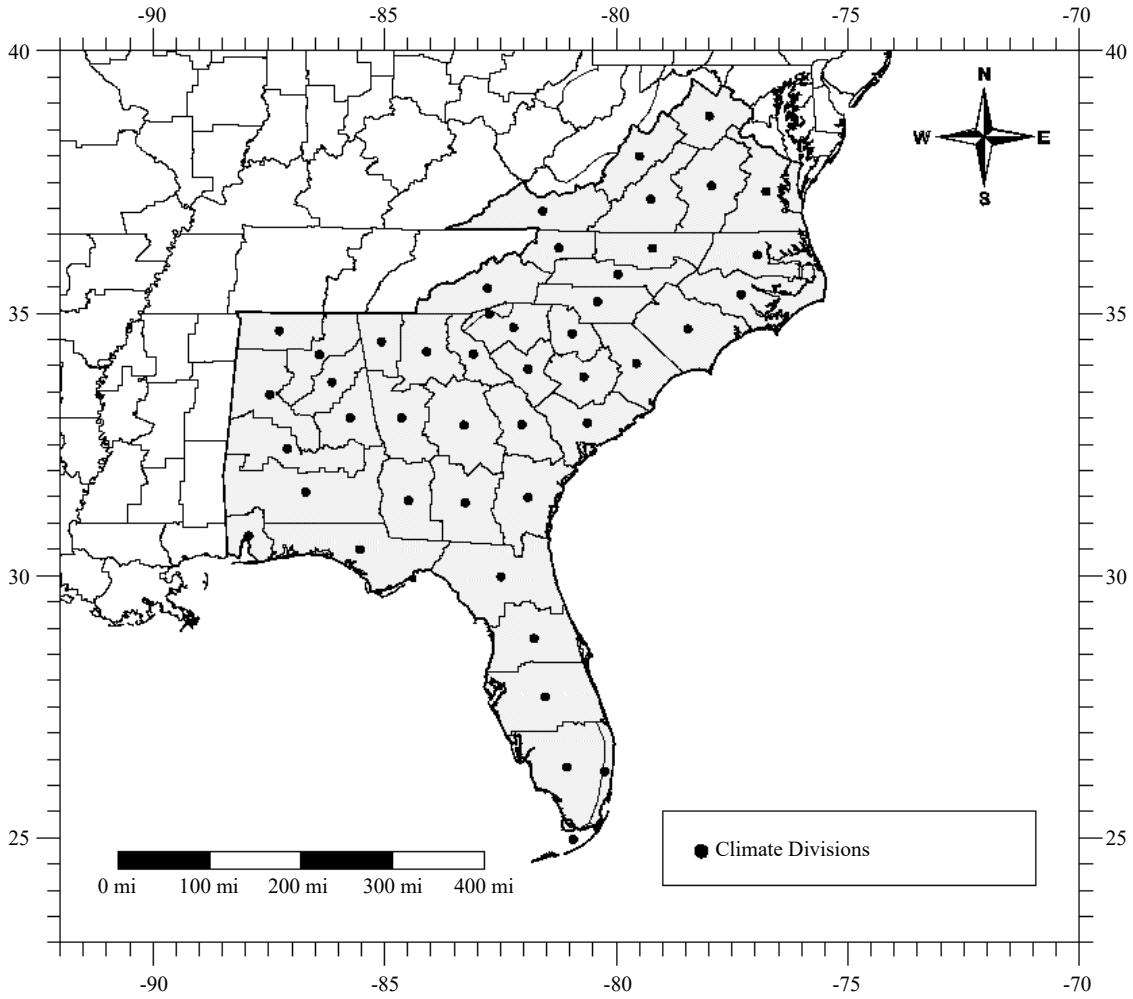

Figure 1. Climate divisions.

3. Method

The methodological approach for un¬derstanding teleconnection patterns consists of empirical orthogonal teleconnection [30], cross correlation analysis [20], composite analysis, and harmonic analysis [9,15,31,32]. Also, Kalaycı et al. [33] employed spectral analysis to identify the regional-scale interannual variability of precipitation and streamflow and some periodicities associated with the warm phase of Southern Oscillation. For investigating the spatiotemporal extent to which LISO affect precipitation patterns over the southeastern of the United States, an empirical method [9], annual cycle and cross correlation analyses are employed with some changes and additions. As shown in Figure 2, the specific procedure of this analysis consists of mainly three steps, namely, data processing, spatial and temporal analyses, and comparative statistical assessment. In the first step, the original raw data are transformed into appropriate data formats, e.g., ranked percentile, modular coefficients, and categorized SOIs. In the second step, candidate and core regions are determined using composite and harmonic analyses. Then, in the last step, LISO–related precipitation signals are compared using lag cross-correlation and annual cycle analyses.

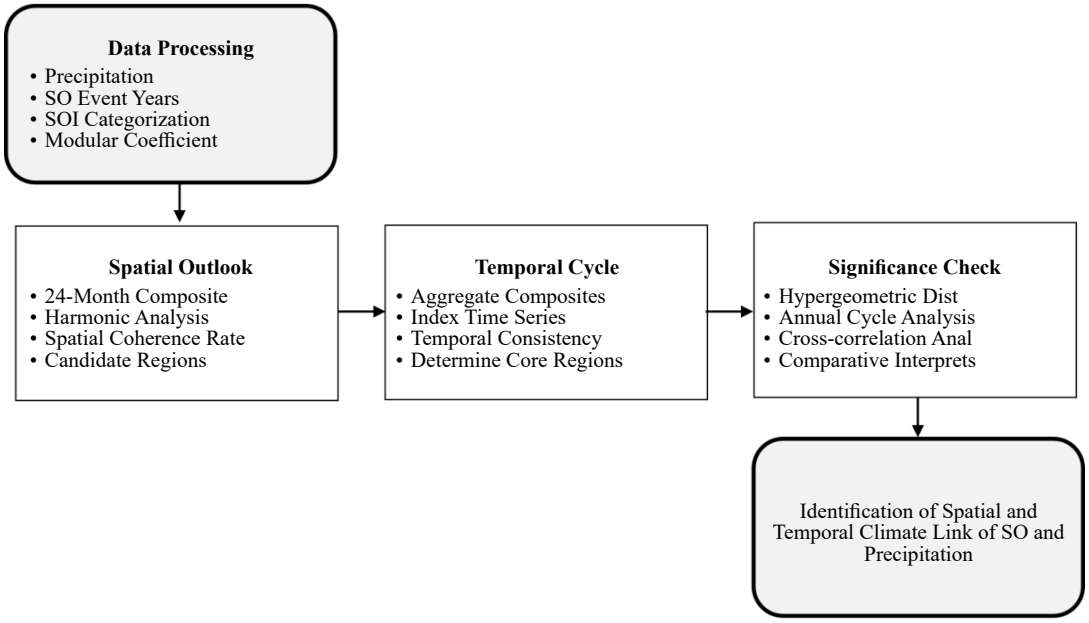

Figure 2. Flowchart of methodology.

Monthly precipitation time series are transformed into modular coefficients for carrying out annual cycle analysis. These modular coefficients remove the effects of dispersed variance and mean values. The precipitation data are expressed as percentages for the annual mean values. The modular coefficient data are calculated by the rate of each monthly precipitation value to the monthly average value for the entire data. It places all divisions on a same cycle with unchangeable condition of the cyclic feature of the values at the same time. In this present study, lag cross-correlation coefficients are computed for precipitation data and categorized SOI time series on a seasonal basis. To do this, four seasonal precipitation and SOI time series are formed by averaging three-month values. The four seasons consist of December-February (DJF), March-May (MAM), June-August (JJA), and September-November (SON). Then, all SOI values are categorized into five levels based on the magnitudes of individual data [20]. The five categories of the SOI values are strong warm phase, weak warm phase, normal phase, weak cold phase, and strong cold phase. On the other hand, the seasonal precipitation data are converted into percentile ranked probability time series to remove periodicities in precipitation time series and to deal with the disparities among climate divisions. The percentile ranked probability values are based on Weibull plotting position formula. All precipitation values are ranked in ascending order and then divided by n+1 (n: size of data).

Monthly precipitation percentile rank composites on 24-month basis are computed for each climate division, starting with the July preceding the event, continuing through the June following the event year, for the LISO. The July preceding the event is designated as Jul (-), while the June following the event year is expressed as Jun (+) as shown in figure 3. The composite for each climate division is then fitted with the first harmonic of an idealized 24-month LISO cycle (either warm or cold episodes). This method assumes one precipitation peak (or trough) during the duration of a LISO event and that the LISO is phase locked to the annual cycle. A 24-month compositing period was chosen since this defines the period during which one phase of the LISO goes through its entire cycle [4]. In the first harmonic cycle, the amplitude represents magnitude of the LISO-related precipitation signals, and the angular phase indicates time of the peak anomaly from the mean value (Figure 4). The formula of the harmonic fits are as follows [34].

$$y_t = \bar{y} + \sum_{i=1}^{n/2}\left\{c_i \cos\left[\frac{2\pi it}{N} - \beta_i\right]\right\} = \bar{y} + \sum_{i=1}^{n/2}\left\{A_i \cos\left[\frac{2\pi it}{n}\right] + B_i \sin\left[\frac{2\pi it}{n}\right]\right\} \tag{1}$$

$$A_i = \frac{2}{n}\sum_{t=1}^{n} y_t \cos\left(\frac{2\pi it}{n}\right), B_i = \frac{2}{n}\sum_{t=1}^{n} y_t \sin\left(\frac{2\pi it}{n}\right), C_i = \left(A_i^2 + B_i^2\right)^{0.5} \tag{2}$$

$$\beta_i = \tan^{-1}\frac{B_i}{A_i}\left(A_i \rangle 0\right), \frac{\pi}{2}\left(A_i = 0\right), \tan^{-1} \pm \left(A_i \langle 0\right) \tag{3}$$

where y_t is monthly precipitation value, $\underline{y}$ is the mean precipitation value, t is time of observation, i is number of harmonic fits, n is sample size, C_i is amplitude of the harmonic curve (magnitude of curve), β_i is time of harmonic peak (temporal phase of curve), and A_i and B_i are Fourier coefficients.

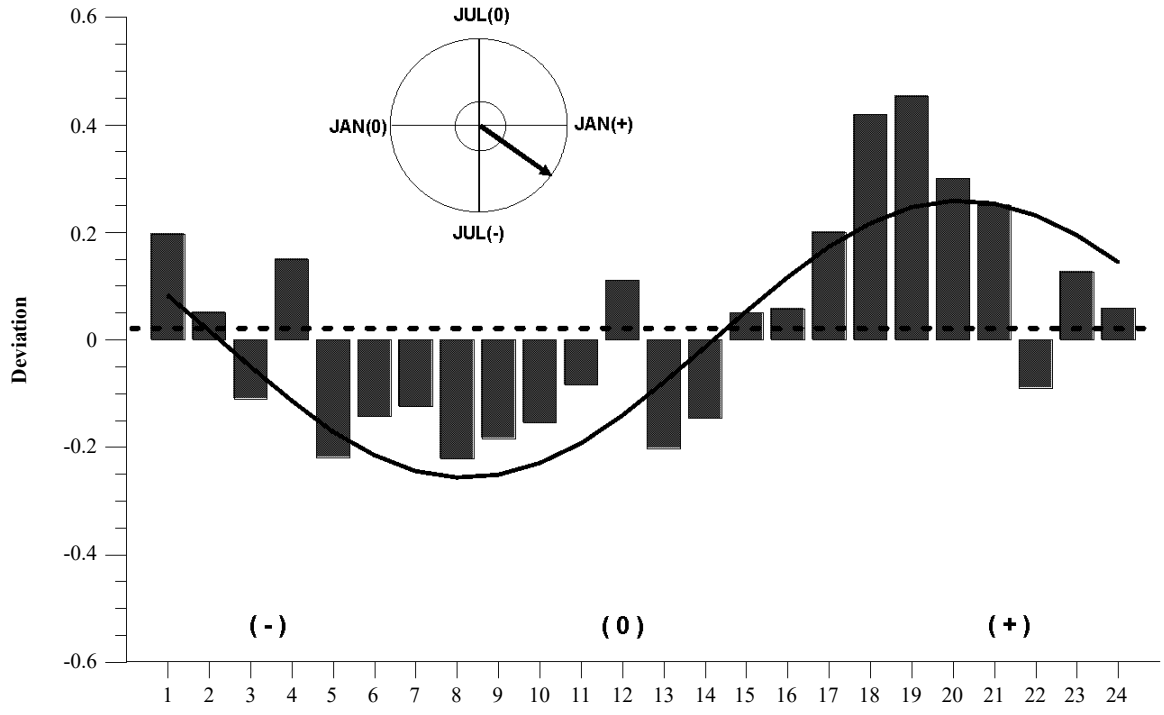

Figure 3. A first harmonic fit to the precipitation SO composite for the climate division. The amplitude and the phase of the first harmonic are presented as a harmonic dial.

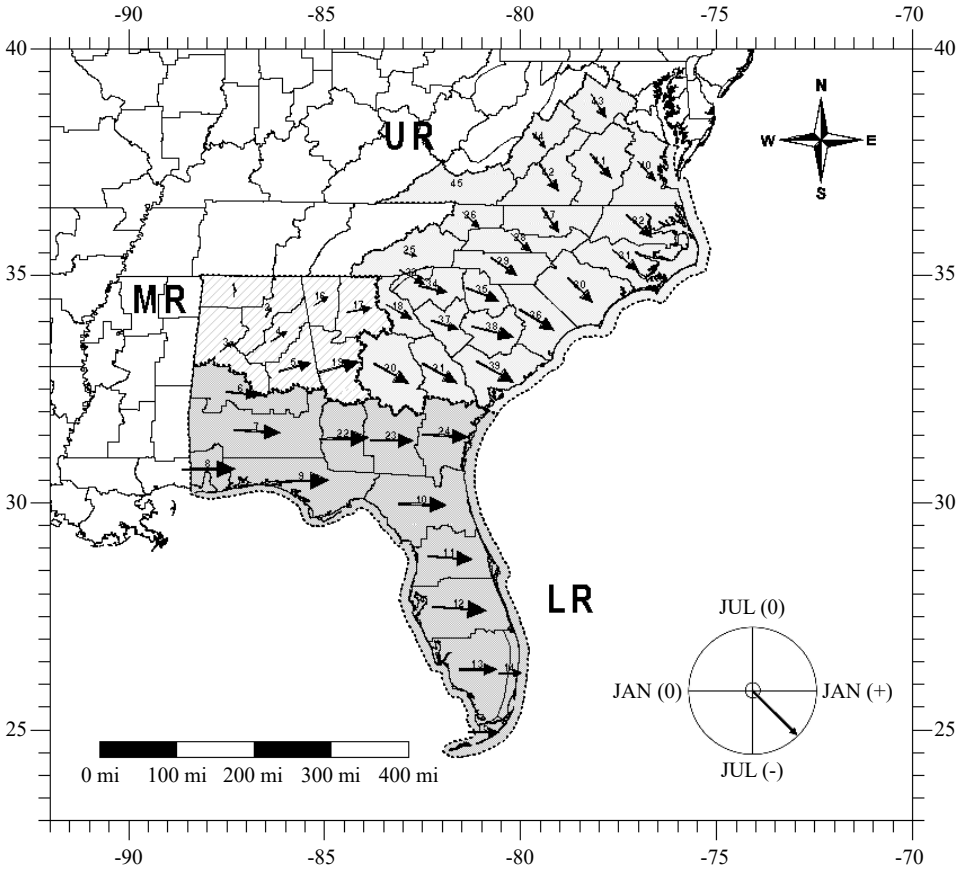

Figure 4. Harmonic dial map based on the first harmonic of the 2-year SO composites. Scale for the direction of arrows: south, July (−); west, January (0); north, July (0); and east, January (+). The magnitude of arrows is proportional with the amplitude of the harmonics.

After the climate division composites are fit with a 24-month harmonic, the amplitude and phase of the curve is plotted as a vector for each station. In the analysis convention chosen here, the vector points toward the positive part of the cycle, that is, wetter-than-normal precipitation. It is only after examining the composites, described below, that the actual sign of the LISO-precipitation relationship can be determined. This study is concerned with regional areas of the southeastern United States that exhibit strong LISO-precipitation relationships over periods of many months. Therefore, individual, or isolated, climate division that shows strong apparent relationships or areas that have short-time scale relationships are not considered for further study.

Plotting the harmonics as vectors on a map provides a method to spatially identify candidate geographic areas that appear to have a coherent LISO-precipitation response. We attempted to choose the largest areas of coherent LISO-precipitation response, where the "coherence" is estimated through the computation of the ratio of the magnitude of the average vector to the arithmetic average value of the vector magnitudes.

$$SC = \frac{\left[\left(\sum v_{\cos\theta}\right)^2 + \left(\sum v_{\sin\theta}\right)^2\right]^{1/2}}{\sum V} \tag{4}$$

where the numerator is the average vector magnitude of all harmonic vectors within the candidate regions, the denominator is the arithmetic average value of the vector magnitudes, θ is angle of the vector, and V is magnitude of the vector. The analysis that follows is limited to areas for which values of the coherence were equal to or greater than 0.80 [9]. This eliminates from the analysis regions that contain harmonic vectors with large amplitudes at a few stations which have little consistency in phase, i.e., low coherence.

Aggregate composites are formed to detect the LISO-related precipitation signal seasons. These signal seasons represent apparently consistent precipitation responses to the extreme LISO forcing. All LISO composite values in a candidate region are averaged and plotted on a 24-month period to cover the entire LISO cycle and identify accurately the signal season. One season within the aggregate composite is found by detecting a group of values showing more than five consecutive months with the same sign. The event year and the following year are regarded as the responding period of LISO phenomena, considering the distance between the study area in midlatitude and the LISO area in the Pacific Ocean.

Index Time Series (ITS) are computed by temporally averaging precipitation values of the signal seasons for the entire years of record and by spatially averaging the precipitation data over the candidate regions. The ITS values are used to quantify the temporal consistency of the LISO impact on precipitation patterns. Temporal consistency rates for the candidate regions are computed using the rate of the number of years exhibiting LISO signal in ITS to the number of all LISO event years. These temporal consistency rates are the determinant of the core regions showing consistent precipitation responses to LISO phenomena. In addition, extreme precipitation events are examined in association with LISO forcing as demonstrated by Ropelewski and Halpert [9]. They investigated climate linkage between LISO events and extreme precipitation occurrences. In the present study, the number of years showing the LISO-related extreme precipitation signal is counted during the signal season. To assign the highest and lowest levels of the extreme events, the ITS time series are ranked from the highest value to the lowest value, normalized by the entire data, and transformed to the probability time series [15]. The highest value is assigned to the probability of 80% ITS, while the lowest value is assigned to the probability of 20% ITS.

Hypergeometric distribution test is employed to assign the significance level of the LISO-precipitation correlation. Haan [35] conducted the hypergeometric distribution test calculating “the cumulative probability that at least m successes are obtained in n trials from a finite population of size N containing k successes”. A cumulative probability computed from the hypergeometric distribution gives an occurrence significance level of the relationship previously defined for both extreme phases of the LISO. Kahya and Dracup [15] used hypergeometric test in terms of average value and high-low extreme events. In the present test, two cases (I and II) are considered according to the definition of a success. In case I, a success is defined as the occurrence of years that an ITS value associated with LISO events is lower than the median, while in case II, a success is defined as the occurrence of year in which an ITS values associated with SO events falls into the lower 20% of the distribution.

Annual cycle analysis is used as a comparative interpretation of two LISO effects on the precipitation anomaly from the perspective of magnitude and annual trend of the signal. Monthly precipitation time series are transformed into modular coefficients for carrying out annual cycle analysis. These modular coefficients remove the effects of dispersed variance and mean values. The precipitation data are expressed as percentages for the annual mean values. The modular coefficient data are calculated by the rate of each monthly precipitation value to the monthly average value for the entire data. This annual cycle plots make it possible to determine whether the extreme phases of SO events modulate precipitation increasingly.

Cross-correlation coefficients are calculated on a seasonal basis to compare the positive and negative LISO-related precipitation signals. Five categorized SOI data sets as SO index are correlated with the monthly precipitation time series expressed by percentile ranked probability. The resulting correlation coefficient values indicate the magnitude and sign of the relationship between the precipitation patterns and the LISO forcing on a seasonal basis. More detailed explanation of the data conversion and correlation procedure was described in the first section of data processing.

4. Results and Discussion

4.1 *Precipitation response to LISO*

For 29 LISO episodes, the composite and harmonic analyses were performed on the monthly precipitation data. The vectorial map for precipitation indicates three regions of the southeastern United States that appear to have a coherent LISO response. The candidate regions are the North Region (UR), the Middle Region (MR), and the South Region (LR). As shown in Table 2, composite precipitation indices for each region indicate that the UR, MR, and LR regions may have a LISO-related response. The precipitation composites for the three regions show clearly defined wet season within the LISO cycle and thus they are explained in detail for further consideration in this analysis.

Table 2. List of the low index phase of southern oscillation (LISO) years

Region	Season	Coherence	Episode	Consistency
UR	Nov (0) – Mar (+)	0.94	22	76%
MR	Sep (0) – Jan (+)	0.94	22	76%
LR	Nov (0) – Mar (+)	0.99	24	83%

The time series of the November (0) to March (+) precipitation indices averaged over all stations in the UR region (Figure 5) illustrates the notable consistency in the precipitation with respect to the LISO in this part of the southeastern United States. This season showed above normal, i.e., greater than the average precipitation for 22 out of 29 LISO events. Further, of the 25 occurrences of index values equal to or greater than the highest ITS limit (80%), 11 of them occurred in association with LISO (Figure 6). Only one of the occurrences in the lowest ITS limit (20%) was associated with LISO. The spatial coherence and temporal consistency were 0.94 and 0.76.

Time series of the MR region precipitation index based on the climate division data for the September (0) to January (+) season (Figure 5) shows above normal precipitation for 22 out of the 29 LISO events. While the index shows values of greater than or equal to the highest ITS limit (80%) for 10 of the LISO years, positive values of the same magnitude or greater also occur during 14 non-LISO-related years (Figure 6). Only one of the LISO-related seasons in the MR area fall into the lowest, or driest, ITS limit (20%). The spatial coherence and temporal consistency were 0.94 and 0.77.

Time series of the precipitation index for the LR region, November (0) to March (+) in Figure 5, shows another example of conclusive result. 24 out of 29 LISO seasons are associated with above median precipitation in the time series based on the climate division data. Since the probability of getting 24 observations of the same sign strictly by chance is relatively low, the result is statistically significant. The precipitation index exceeded the 80% index value with 13 LISO episodes, and none of the occurrences in the lowest ITS limit (20%) was associated with LISO (Figure 6). The spatial coherence and temporal consistency were 0.99 and 0.83. Thus, it appears that LISO is a reliable discriminator of the precipitation anomalies of the LR region.

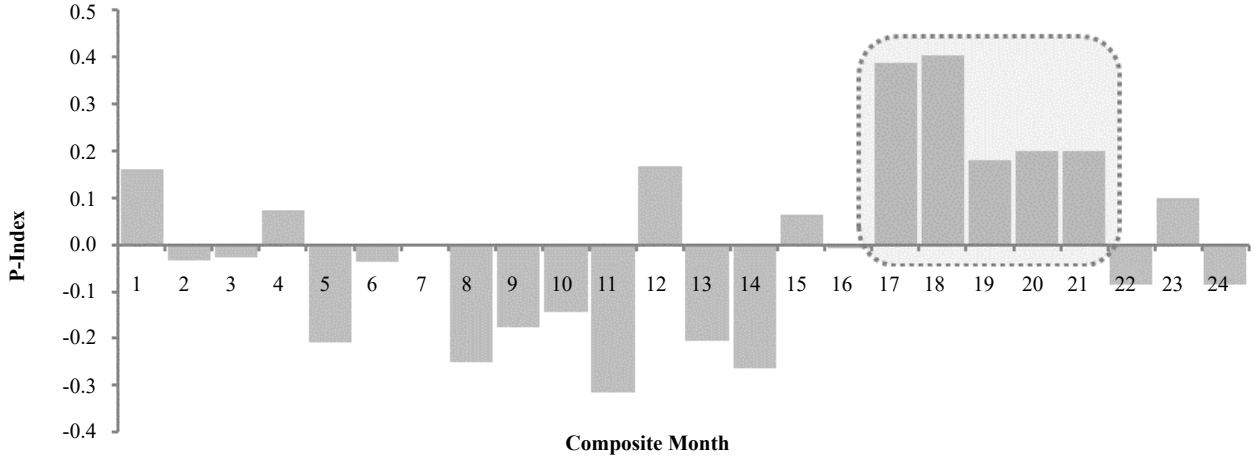

(a) UR

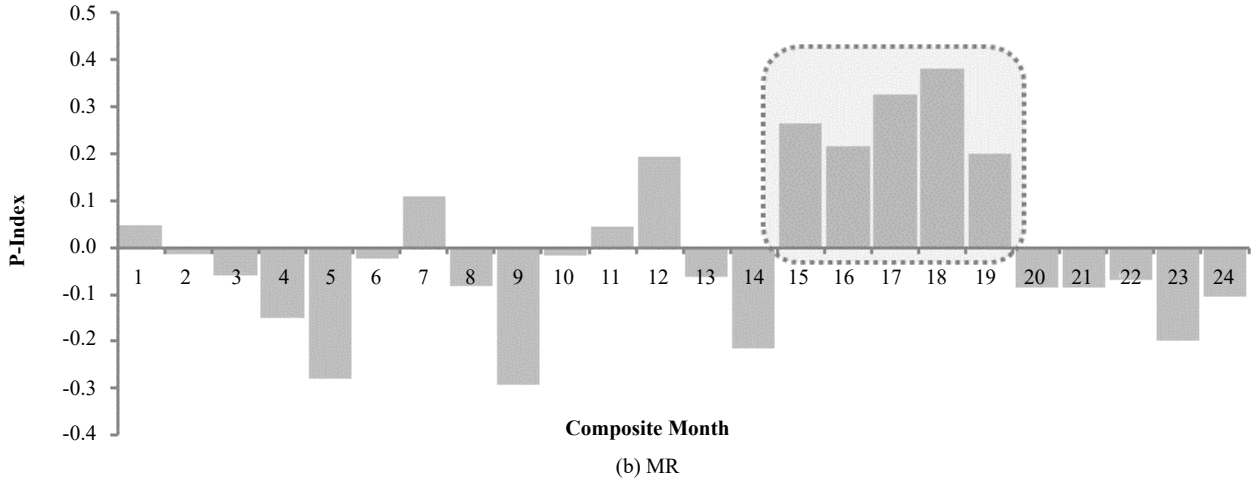

(b) MR

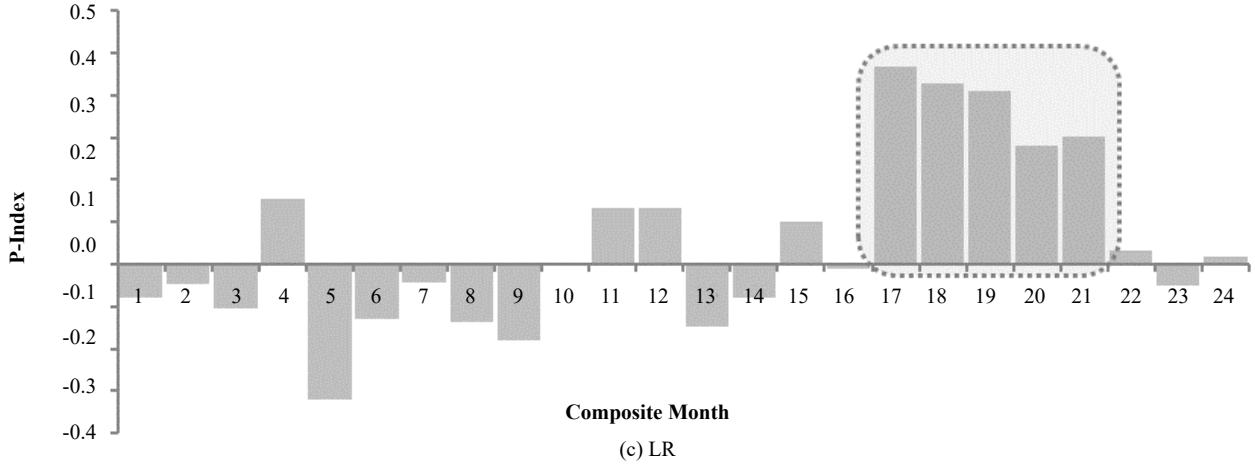

(c) LR

Figure 5. SO aggregate composite for the candidate UR, MR, and LR region. The dashed line box delineates the season of possible SO-related responses

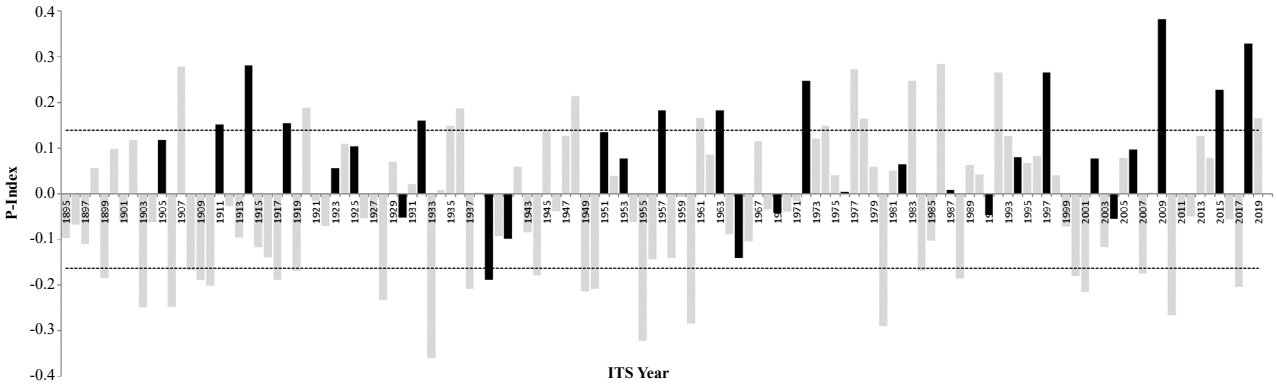

(a) UR

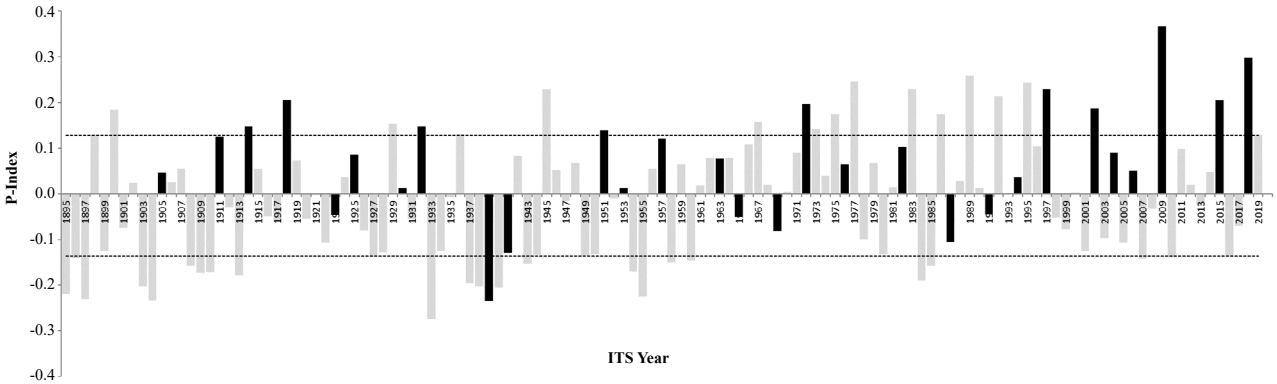

(b) MR

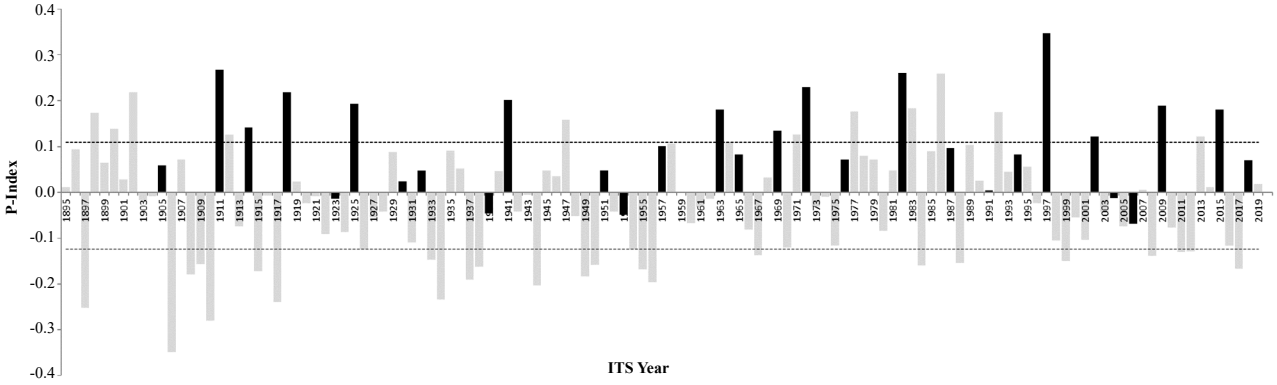

(c) LR

Figure 6. The index time series for the UR, MR, and LR regions for the season previously detected. SO years are shown by solid bars. The dashed horizontal lines are the upper (80%) and lower (20%) limits for the distribution of ITS values.

4.2 *Seasonal and Annual Variation*

The probability that wet (dry) season occurs at random during the LISO event years was tested by the hypergeometric distribution (Table 3). In case I, the application of the hypergeometric distribution model results in a very low level of probability of occurrence by chance (less than 0.004) for LISO events. In case II, the probability is also very low for the LISO events. The extreme wet precipitation conditions appear to be almost exclusively related to LISO events in the 125-yr period. Overall results in Table 3 are also consistent with the high confirmation rates (76-83% in Table 2) for temporal consistency of the signals. All of this implies that the relationship depicted in the aggregate composites is probably due to nonrandom forcing mechanism, i.e., the tropical thermal anomalies.

Monthly precipitation time series are transformed into modular coefficients for carrying out annual cycle analysis. From this resulting series, LISO composites are formed and plotted along with the regional annual cycle (Figure 7). For a typical precipitation behavior during LISO events, a suppressed precipitation of the annual cycle during the event year is followed by an enhanced precipitation of the annual cycle from the end of event year to the beginning of the following year. This enhancement of magnitudes is roughly concurrent with the previously detected wet signal seasons in three core regions. In summary, the resulting findings suggest that the tropical heating anomalies modulate the annual precipitation cycle within the southeastern United States by increasing.

Table 3. Results of significance assessment by hypergeometric distribution test

Case	Region	N	n	m	Prob.
A	UR	125	63	29	0.002
	MR	125	66	29	0.004
	LR	125	61	29	0.000
B	UR	125	25	11	0.002
	MR	125	25	10	0.008
	LR	125	25	13	0.000

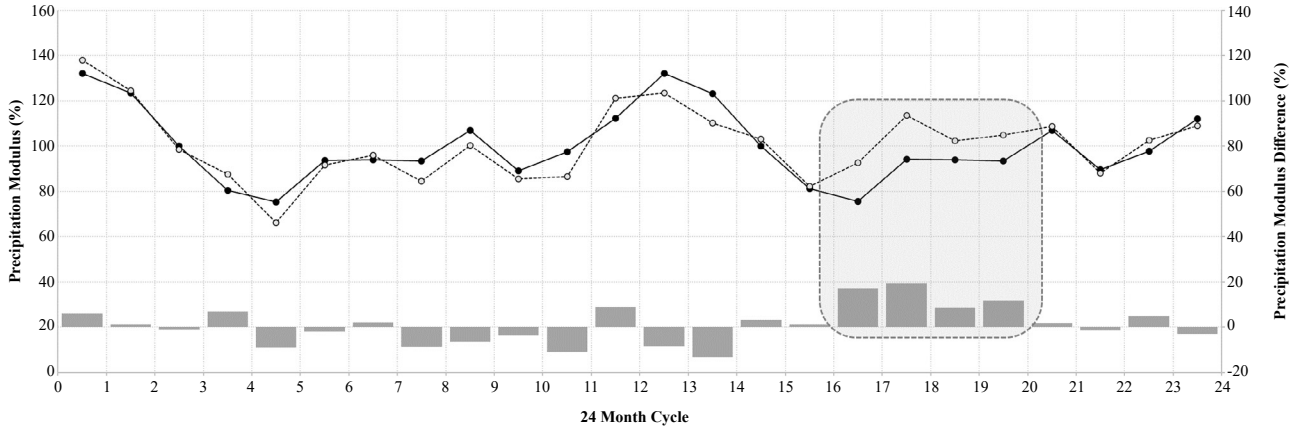

(a) UR

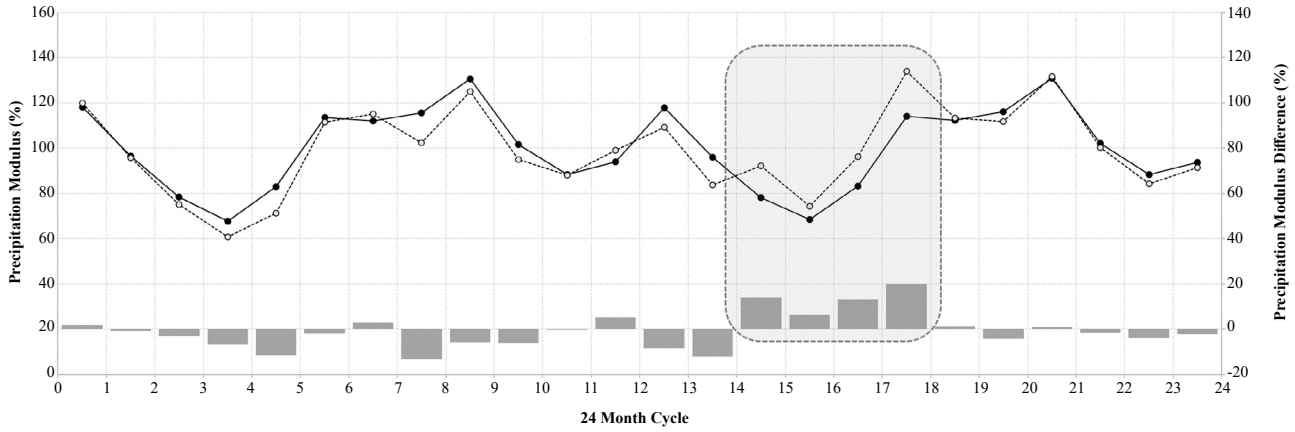

(b) MR

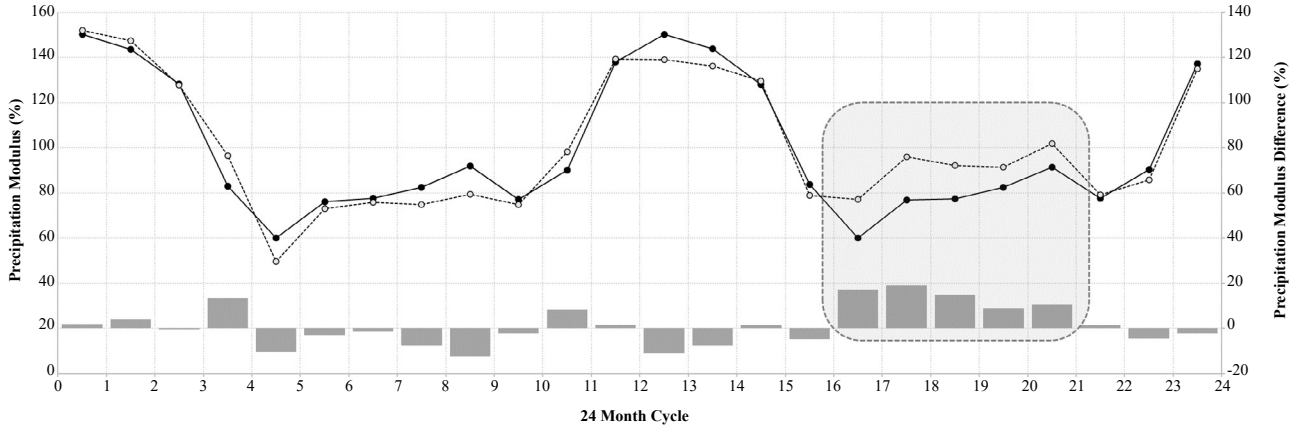

(c) LR

Figure 7. The SO composite cycles (shown by dashed line) and annual cycles (shown by solid line) of the UR (upper), MR (middle), and LR (lower) regions, based on modular coefficients. Dashed boxes indicate the beginning and end months of the SO signal season. The tropical thermal forcing modulates seasonal precipitation cycle by increasing for the signal seasons, i.e., November to February (UR), September to December (MR), and November to March (LR).

Table 4 displays the results of calculating cross-correlation coefficients. These values represent intensity and sign of the correlation between the LISO phenomena and precipitation anomalies. This correlation analysis is conducted for large-scale climate indicator (LISO index) and the seasonal precipitation anomalies, which use five categorized SOI data sets and percentile ranked probabilities, respectively. As a result, the seasonal precipitation anomalies were significantly correlated with both extreme phases of SO at 0.05 significance level. The highest positive correlation coefficient values are shown in the lag-2 and lag-3 cases over the three core regions for the strong warm phase SOI condition. For the strong cold phase SOI condition, the highest negative correlation coefficient values are found at all core regions with lag-2 and lag-3 cases. As a result, the stronger warm and cold phases of SOI, the more and less precipitation with lag time 2 and 3 seasons over the southeastern United States.

Table 4. Results of cross-correlation coefficient with respect to regions.

Core Region	Strong Warm Phase					Strong Cold Phase				
	lag-0	lag-1	lag-2	lag-3	lag-4	lag-0	lag-1	lag-2	lag-3	lag-4
UR	0.08	0.23	**0.61**	**0.86**	0.12	**0.35**	-0.02	**-0.45**	**-0.46**	0.3
MR	-0.29	0.23	**0.69**	**0.79**	0.21	**0.44**	0.25	**-0.65**	**-0.53**	0.15
LR	-0.01	0.17	**0.46**	**0.32**	0.29	0.21	0.08	**-0.59**	**-0.41**	-0.03

4.3 *Discussions*

As shown in Figures 4 to 6, the results of this study show positive precipitation response to the LISO events at the UR, MR, and LR regions during early fall (0) to spring (+) seasons. Especially, amplitude of the positive precipitation departure of LISO year at the SR region is even higher than that of non-LISO year. The precipitation response in the southeastern United States to the southern oscillation is consistent with Ropelewski and Halpert [9], Douglas and Englehart [8]. Ropelewski and Halpert [9] stated that the precipitation response to SO may be more easily explained in terms of direct or shorter range effects related to the enhanced subtropical jet stream and warmer than normal surface water over the Pacific. Douglas and Englehart [8] suggested that the SO-related precipitation signal may be an indication of a more direct link to SO forcing than a Pacific North American teleconnection pattern (PNA). Active SO-related convection is typical in the equatorial Pacific, south of the southeastern United States. This convection has been linked to stronger than normal westerlies in the southern parts of the United States including Gulf of Mexico (e.g., 200 mb SO composites in Arkin [36]) and, hence, a tendency for more frequent storms and precipitation in the southeastern United States. This possible direct link to the SO-related forcing may account for the consistent precipitation response over the southeastern US. Rasmusson and Wallace [37] found a strengthened subtropical jet stream displaced southward from its normal position during the mature phases of SO event (1982-1983). This pronounced intensification of the jet stream drove numerous winter storms causing flooding events in the southern parts of the United States. Additionally, they indicated that this region has shown abnormal wet conditions associated with past SO events. During the SO event years, the persistent occurrence of warm and cold sea surface temperatures over the central/eastern equatorial Pacific triggers large-scale atmospheric fluctuations in the middle latitude based on complex air-sea coupled interactions. As a result, these LISO-related middle latitude circulations excite abnormal precipitation patterns over the southeastern United States.

Ropelewski and Halpert [9] documented the climatic links between the extreme southern oscillation and precipitation anomalies over North America and showed the SO-related precipitation signals. The analysis showed that above normal precipitation was associated with ENSO in the 18 out of 22 cases (81%) in the “season” starting with October of the event year to March of the following year for an area of the southeastern United States and northern Mexico. Their core region is consistent partially with the Lower Region (LR) in the present study. The present study showed that time series of the precipitation index for the LR region, November (0) to March (+) and 24 out of 29 events were associated with above median precipitation in the time series based on the climate division data. The spatial coherence and temporal consistency were 0.99 and 0.83.

In addition, Kahya and Dracup [14] examined the relationship between the extreme phase of Southern Oscillation and unimpaired streamflow over the contiguous United State. They found that the southern US region shows statistically significant correlation between tropical thermal forcing and streamflow patterns. The signal season of December (0) to April (+) was considered as a time period for strong teleconnection and 6 out of 9 event occurrences (67%) confirmed the wet season. The spatial coherence rate was 0.88. The signal season and spatial pattern are consistent with those of the LR region in the present study. The signal season for the above normal precipitation was November of the event year to March of the following year and 24 out of 29 event occurrences (83%) confirmed the wet signal season. The spatial coherence rata was 0.99.

5. Summary and Conclusions

Teleconnection between two phases of SO thermal forcing and monthly precipitation anomaly in the southeastern United States was investigated using a set of empirical and statistical analyses, such as harmonic analysis, annual cycle composites, and cross-correlation analysis. From the results of vectorial mapping through composite and harmonic analyses, the southeast climate region is classified into three core regions designated as Upper Region (UR), Middle Region (MR), and Lower Region (LR). They showed high levels of spatial coherence and temporal consistency with notable spatial range and amplitude of the precipitation response to LISO phenomena. The main conclusions are outlined as follows.

During the LISO events, the monthly precipitation anomalies are above normal in the UR, MR, and LR regions. For the three core regions, the Nov (0) to Mar (+), Sep (0) to Jan (+), and Nov (0) to Mar (+) are the signal seasons showing the noticeable consistency in precipitation in association with the warm LISO forcing. The spatial coherence of the three core regions for LISO events ranges from 0.94 to 0.99 and the temporal consistency are between 0.76 and 0.83. Especially, the LR core region showed the highest magnitude of the positive precipitation departure for the LISO years.

From the results of annual cycle analysis, the tropical heating anomalies of sea surface temperature modulate the annual precipitation cycle within the southeastern United States by increasing. The highest positive (negative) correlation coefficient values are shown in the lag-2 and lag-3 cases over the three core regions for the strong warm (cold) phase SOI condition. That is, the stronger SOI forcing, the more and less precipitation with lag time 2 and 3 seasons over the southeastern United States. Consequently, it is concluded that middle latitude precipitation responses to the LISO phenomena are detectable over the southeastern United States.

References

[1] Walker, G.T., 1923. Correlation in seasonal variations of weather, V III, A preliminary study of world weather, *Memoirs of the India Meteorological Department,* 24, 75-131.

[2] Walker, G.T., Bliss, E.W., 1932. WORLD WEATHER V - *Royal Meteorological Society*, 4 (36), 53-84.

[3] Berlage, H.P., 1966. The Southern Oscillation and world weather. Mededglingen en Verhandelingen Koninklijk Nederlands Meteorologisch Instituut No. 88, pp. 152.

[4] Rasmusson, E.M., Carpenter, T.H., 1983. The relationship between eastern equatorial Pacific sea surface temperatures and rainfall over India and Sri Lanka. *Monthly Weather Review*, 111, 517-528.

[5] Ropelewski, C.F., Halpert, M.S., 1987. Global and regional scale precipitation patterns associated with the El Niño/ Southern Oscillation. Monthly Weather Review, 115, 1606-1626.

[6] Ropelewski, C.F., Halpert, M.S., 1989. Precipitation patterns associated with the high index phase of the southern oscillation. *Journal of Climate*, 2, 268-284.

[7] Westra, S., Alexander, L.V., Zwiers, F.W., 2013. Global increasing trends in annual maximum daily precipitation. *Journal of Climate*, 26: 3904-3918.

[8] Douglas, A.E., Englehart, P.J., 1981. On a statistical relationship between autumn rainfall in the central equatorial pacific and subsequent winter precipitation in Florida, *Monthly Weather Review*, 109, 2377-2382.

[9] Ropelewski, C.F., Halpert, M.S., 1986. North American precipitation and temperature patterns associated with El-

Niño-Southern oscillation (ENSO), *Monthly Weather Review* ,114, 2165-2352.
[10] Cayan, D. R., Peterson, D. H., 1989. The influence of North Pacific atmospheric circulation on streamflow in the West, in Aspects of climate variability in the Pacific and the Western Americas. *American Geophysical Union · Geophysical monograph*, 55, 375-397.
[11] Redmond, K.T., Koch, R.W., 1991. Surface climate and streamflow variability in the western United States and their relationship to large circulation indices, *Water Resources Research*, 27(9), 2381-2399, 1991.
[12] Cayan, D. R., Webb, R. H., 1992. El Niño/Southern Oscillation and streamflow in the western United States, in El Niño: Historical and Paleoclimatic Aspects of the Southern Oscillation, edited by Diaz, H. F. and Markgraf, V., Cambridge University Press, 29-68.
[13] Diaz, H. F., Kiladis, G. N., 1993. El Niño/Southern Oscillation and streamflow in the western United States, in El Nitio: Historical and Paleoclimatic Aspects of the Southern Oscillation, edited by Diaz, H. F. and Markgraf, V., Cambridge University Press, 8-28.
[14] Kahya, E., Dracup, J.A., 1993. U.S. Streamflow Patterns in Relation to the El Nino/Southern Oscillation. *Water Resources Research*, Vol. 29, No 8, 2491-2503.
[15] Kahya, E., Dracup, J.A., 1994. The influences of Type 1 El Niño and La Niña events on streamflows in the Pacific southwest of the United States. *Journal of Climate*, 7: 965-976.
[16] Grimm, A. M., Ferraz, S.E.T., Gomez, J., 1998. Precipitation Anomalies in Southern Brazil Associated with El Niño and La Niña Events, *Journal of Climate*, 11, 2863-2880.
[17] Chiew, F. H. S., McMahon, T. A., Dracup, J. A., Piechota, T., 1994. El Niño/Southern Oscillation and the streamflow patterns in south-east Australia, Civil Engineering Transactions. Institution of Engineers, Australia, CE36 (4), 285-291.
[18] Karabörk, M.Ç., Kahya, E., 2003. The teleconnections between extreme phases of Southern Oscillation and precipitation patterns over Turkey, *International Journal of Climatology*, 23, 1607-1625.
[19] Kahya, E., Karabörk, M. C., 2001. The analysis of El Niño and La Niña signals in streamflows of Turkey. *International Journal of Climatology*, 21(10), 1231-1250.
[20] Jin, Y.H., Kawamura, A., Jinno, K., Berndtsson, R., 2005. Quantitative relationship between SOI and observed precipitation in southern Korea and Japan by nonparametric approaches. *Journal of Hydrology*, 301, 54-65.
[21] Chandimala, J., Zubair, L., 2007. Predictability of streamflow and rainfall based on ENSO for water resources management in Sri Lanka. *Journal of Hydrology*, 335, 303-312.
[22] Power, S.B., Haylock, M., Colman, R., Wang, X., 2006. The predictability of Interdecadal changes in ENSO activity and ENSO teleconnection. *Journal of Climate*, 19: 4755-4771.
[23] Cai, W., Rensch, P.V., Cowan, T., 2011. Teleconnection pathways of ENSO and the IOD and the mechanisms for impacts on Australian rainfall. *Journal of Climate*,24: 3910-3923.
[24] Zhang, Q., Xu, C. Y., Jiang, T., and Wu, Y., 2007. Possible influence of ENSO on annual maximum streamflow of the Yangtze River, China, *Journal of Hydrology*, 333, 265-274.
[25] Kashid, S.S., Ghosh, S., Maity, R., 2010. Streamflow prediction using multi-site rainfall obtained from hydroclimatic teleconnection, *Journal of Hydrology*, 395, 23-38.
[26] Lee, J.H., Julien, P.Y., 2016. Teleconnections of the ENSO and South Korean precipitation patterns. *Journal of Hydrology*, 534, 237-250.
[27] Lee, J.H., Julien, P.Y., 2017. Influence of the El Niño/Southern Oscillation on South Korean streamflow variability. *Hydrological Processes*, 31, 2162-2178.
[28] Lee, J.H., Julien, P.Y., Jorge A. R., Kim, T.W., 2019. Variability, teleconnection, and predictability of Korean precipitation in relation to large scale climate indices. *Journal of Hydrology*, 568, 12-25.
[29] Wang, L., Yang, Z., Gu, X., Li, J., 2020. Linkages Between Tropical Cyclones and Extreme Precipitation over China and the Role of ENSO, *International Journal of Disaster Risk Science*, 11, 538-553.
[30] Klingaman, N.P., Woolnough, S.J., Syktus, J., 2013. On the drivers of inter-annual and decadal rainfall variability in Queensland, Australia. International Journal of Climatology 33, 2413–2430.
[31] Lee, J.H., Lee, J., Julien, P.Y., 2019. *"Global Climate Teleconnection with Rainfall Erosivity"*, CATENA, Vol. 167, pp. 28-43.
[32] Lee, J.H., Yang, C.Y., Julien, P.Y., 2020. "Regional rainfall variability associated with large-scale climate

phenomena", *Advances in Water Resources*, Vol. 135, 103462.
[33] Kalaycı, S., Karabörk, M.C., Kahya, E., 2004: Analysis of El Nino Signals on Turkish Streamflow and Precipitation Patterns Using Spectral Analysis. *Fresenius Environmental Bulletin*, Vol. 13, No 8, 719-725.
[34] Wilks, D. S., 1995. Statistical Methods in Atmospheric Sciences. Academic Press, 330-334.
[35] Haan, C.T., 1978. Statistical Methods in Hydrology. Iowa State University Press, Ames, IA, pp. 387.
[36] Arkin, P. A., 1982. The relationship between interannual variability in the 200 mb tropical wind field and the Southern Oscillation. *Monthly Weather Review*, 110, 1393-1404.
[37] Rasmusson, E.M., Wallace, J.M., 1983. Meteorological aspects of the El Niño/southern oscillation. *Science*, 222, 1195-1202.